Preparation, Structural Elucidation, Molecular Weight Determination, and Molecular Recognition of First- and Second-Tier Dendrimer Molecules

Man Singh, Dolly Yadav, Rajesh K. Yadav

Chemistry Research Laboratory, Deshbandhu College, University of Delhi, New Delhi 110019, India

Received 17 December 2007; accepted 20 May 2008
DOI 10.1002/app.28780
Published online 22 August 2008 in Wiley InterScience (www.interscience.wiley.com).

ABSTRACT: 1,3,5-Triglyceratetriazine [first tier (G_1)] and tri(1,3,5-triglycerate) triazine [second tier (G_2)] dendrimers were prepared with 1,3,5-trichlorotriazine and sodium glycerate in a 1 : 3 mass ratio in an ethanolic medium. G_1 and G_2 were amorphous, white, solid substances. Their structures were elucidated with IR, ^{1}H-NMR, and ^{13}C-NMR, and their thermal stability was studied with thermogravimetric analysis. The activation energy was calculated with the Freeman–Carroll model. Densities, viscosities, and surface tensions for 0.01–0.08 mol/kg aqueous solutions increased at 0.01 mol/kg for sodium glycerate, 1,3,5-trichlorotriazine, 1,3,5-triazine triglycerate chloride, G_1, and G_2. These values were measured at 298.15 K. The apparent molal volume, reduced viscosity, and inherent viscosity were calculated from the densities and viscosities, respectively. The data were regressed for the limiting densities, limiting apparent molal volumes, intrinsic viscosities, limiting inherent viscosities, and limiting surface tensions for solute–solvent interactions. The positive limiting apparent molal volume values were noted in the order of G_2 > 1,3,5-triazine triglycerate chloride > G_1 > 1,3,5-trichlorotriazine > sodium glycerate, with weaker hydrophilic intermolecular interactions of G_2. The higher intrinsic viscosity and limiting inherent viscosity values for G_2 implied stronger G_2–H_2O hydrophilic interactions, and the higher limiting apparent molal volume of G_2 indicated slightly higher dynamic conformational changes in comparison with G_1, with stronger structural activities.
 J Appl Polym Sci 110: 2601–2614, 2008

Key words: activation energy; density; hydrophilic polymers; infrared spectroscopy; macromonomers

INTRODUCTION

Currently, many exciting developments in the preparation and characterization of dendritic materials are being driven by more widespread uses, including structural materials, drug loading, microelectronics, coatings, biomedical materials, and building blocks in nanotechnology.[1,2] First discovered in the early 1980s by Tomalia and coworkers,[3] these hyperbranched molecules were called dendrimers because they have treelike or octopus-like structures. The central most part is called the central core, and it has functional groups that lead to bifurcation with suitable molecules, which in turn lead to branching. The terminus of each branch further bifurcates.[4–7] The synthesis of similar macromolecules was independently reported by Newkome's group.[5] The current trends of research in the field of dendrimers demand finer control over the chemistry, morphology, and surface topography on the micrometer and nanometer scales. Thus, a stronger need exists for experimental techniques capable of the highly efficient preparation and characterization of dendritic materials. Many reports have described the synthesis and thermal properties of triazine-based dendrimers, but the preparation of the dendrimers 1,3,5-triglyceratetriazine [TGTA; i.e., the first tier (G_1)] and tri(1,3,5-triglycerate) triazine [i.e., the second tier (G_2)] with glycerol as a branching unit with unique physicochemical properties has yet to be reported. An approach to improving the solubility and processability of heterocyclic dendrimers is enhanced by the use of glycerol and a triazine ring with an unusual combination of properties, such as a high softening temperature, thermal stability, and solubility.[6,7] G_1 and G_2 are biocompatible, are easily synthesized, and support green chemistry. The activation energy and energy barrier have been noted to be higher for 1,3,5-triazine triglycerate chloride (TATC), G_2, and G_1, with maximum optimization for the most stable state and also per Hook's law, according to which asymmetric structures generate different asymmetric stretching frequencies. The IR, NMR, intrinsic viscosity ([η]), limiting inherent viscosity ([η_{inh}]), and density (ρ) data support these structures. G_1 and G_2 may be the best substitutes for drug carriers such as valynomycine, an expensive

Correspondence to: M. Singh (mansingh50@hotmail.com).
Contract grant sponsor: University Grants Commission.

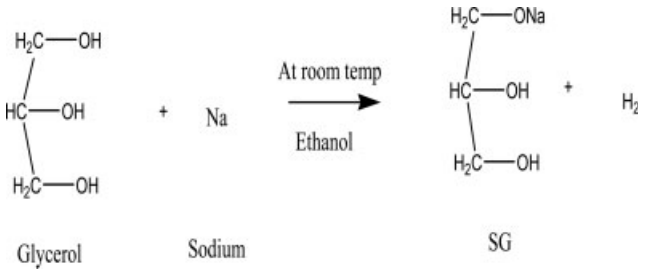

Figure 1 Preparation of SG.

substance whose unfolding dynamics are involved in carrying ions from an aqueous state to a liquid state, whereas in G_1 and G_2, simple hydrophilic and hydrophobic forces are involved. Therefore, our model may be considered quite simplified and many times better than others. These structures are possibly most suitable for hydrophobic and hydrophilic carriers and can transport the ions from an aqueous state to a liquid state. A focus on enriching nanoscience has been facilitated by G_1 and G_2, which do not need further modification of their end groups for the preparation of a variety of nanoparticles, including gold nanoparticles.[8] Also, they can form very interesting biomembranes *in vitro* with the help of gold and silicon atoms. Silicon makes them weakly conducting synthetic biopolymers with tremendous applications in biochips, biophysics, and drug delivery systems. An increase in the branch density with generation leads to internal voids and reactive end groups[9] that provide some unique features such as adhesiveness and an ability to entrap foreign molecules, enzymes, and toxins and carry them to arteries. They also act as scavengers to remove toxic materials. Glycerol, being a very good humectant, enriches G_1 and G_2 so that they behave as water-holding moieties and thus can enrich a variety of industries, including the agricultural industry. G_1 and G_2 can retard leaching by the formation of complexes with metals such as Ca, Na, K, and Mg and enhance the water-holding capacity of soil. They also function as polyelectrolytes with metals.[10] Our dendrimers have significantly lower viscosities than linear polymers,[11] and G_2 shows maximum [η] values with an increase in the molecular mass.[12] Numerous terminal functional groups are responsible for the high solubility, miscibility, high reactivity, and viscosity.[13] The thermodynamic and transport properties of sodium glycerate (SG), 1,3,5-trichlorotriazine (TCTA), G_1, G_2, and TATC are described to illustrate the effects of the compositions on the properties. An attempt is also made to explain specific interactions such as intermolecular, intramolecular, solute–solute, and solute–solvent interactions occurring between the components in these mixtures.

EXPERIMENTAL

Preparation of the G_1 dendrimers

SG

Sodium and glycerol (A.R. Merck) were placed in a 50-mL beaker in a weight ratio of 1 : 1 and stirred constantly at room temperature. The reaction occurred slowly with mild frothing and resulted in a homogeneous, white, solid, and sticky mass (Fig. 1). The reaction was exothermic, raising the temperature of the reaction mixture to 44°C.

Dendrimer G_1

TCTA and SG were placed in a 50-mL beaker in a weight ratio of 1 : 3 and stirred constantly at room temperature in an ethanolic medium. The reaction was a typical substitution reaction in which the glycerate of SG was substituted for the chloride of TCTA to form G_1 and sodium chloride. The reaction was exothermic and raised the temperature to 80°C. The sodium chloride so formed was removed by the addition of ice-cold water to the reaction mixture, which was previously cooled in an ice bath. G_1 still remained in the water as a colloidal mixture, which was then distilled at 97°C to obtain a white, amorphous solid with the structure shown in Figure 2.

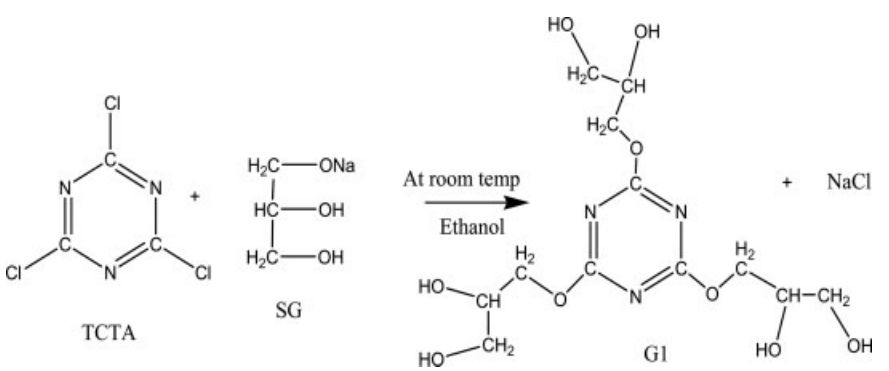

Figure 2 Preparation of dendrimer G_1.

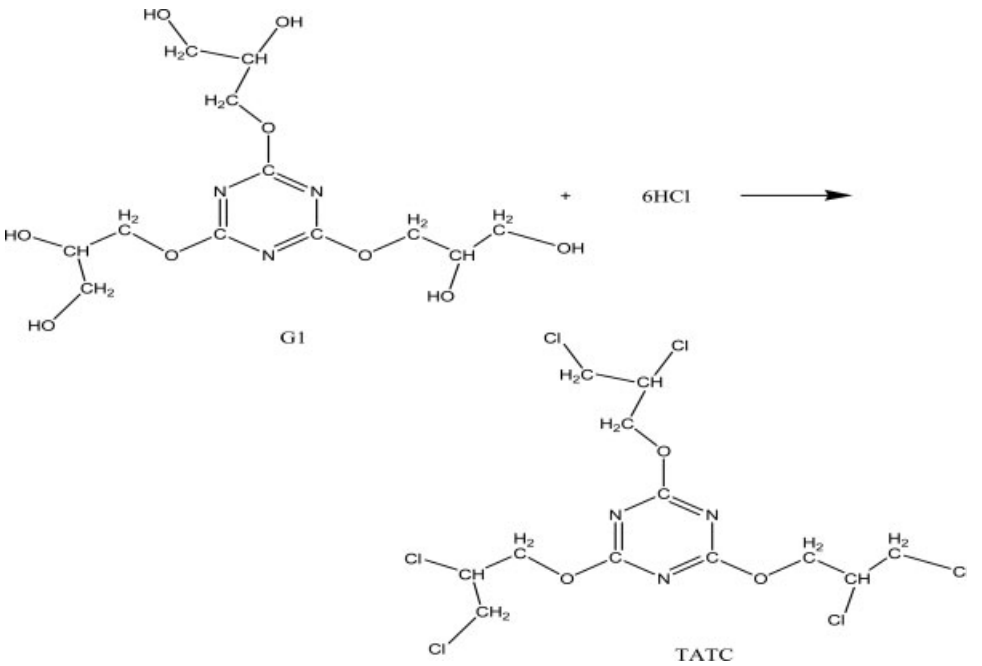

Figure 3 Preparation of TATC.

TATC

The chloride of G_1 was prepared through the heating of G_1 with concentrated HCl in a mass ratio of 1 : 6 in a round-bottom flask in an oil bath for over 4–5 h. G_1 totally disappeared in HCl, and after 2 h, a slight deposition of salt occurred on the sides of the round-bottom flask. Further heating was carried out for 2–3 h, and the solution was left as such overnight; it was then filtered and dried slowly to get a white, crystalline solid of TATC (Fig. 3).

Preparation of G_2

TATC and SG were placed in a round-bottom flask in an alcoholic medium in a mass ratio of 1 : 6 for the preparation of G_2 and NaCl (Fig. 4). The salt so prepared was separated by the addition of ice-cold water to the reaction mixture, which was previously cooled in an ice bath. Further distillation was carried out to recover G_2 from the colloidal mixture.

Physicochemical measurements

The SG, TCTA, G_1, G_2, and TATC solutions were prepared with distilled water (w/w). A bicapillary pycnometer and a survismeter[14] were used for ρ, surface tension (γ), and viscosity (η) measurements. The weights of the empty, solution-filled, and solvent-filled pycnometer were measured with an electronic balance (0.01 mg, model 100 DS, Dhona, Kolkatta, India) for the ρ values.[15] The pycnometer and survismeter were thermostated with a precision of ±0.01°C with a Beckmann thermometer (Germany). The thermostat was kept on a heavy wooden table to avoid jerks and vibrations, and the solutions were thermostated for 25–30 min before the measurements.

Apparatus and procedure

The pycnometer and survismeter were calibrated with aqueous NaCl[16] at 298.15 K, with the thermal stability of the bath better than ±0.01°C. A Hewlett–Packard quartz thermometer calibrated with a gallium temperature standard was used to measure the bath temperature, and the accuracy of the solution concentrations was better than 1×10^{-5} m. The ρ values[17] of water were 0.99705 g/cm^3 at 298.15, 0.99565 g/cm^3 at 303.15, and 0.99404 g/cm^3 at 308.15 K. The calibration was repeated immediately before and after each measurement, and the reproducibility was better than 1×10^{-3} kg/m^3. The viscous flow time with the survismeter[14] was noted with an electronic racer of 1×10^{-2} s, and drop numbers were noted with a drop counter. The kinetic energy correction of the survismeter was calculated to be 1.89×10^{-5} at 298.15 K, with negligible shear and interference in the natural flow.

The densities $\{\rho = [(w - w_e)/(w_0 - w_e)]\rho_0 + 0.0012[1 - (w - w_e)/(w_0 - w_e)]$, where ρ is the solution density; ρ_0 is the solvent density; 1.2 kg/m^3 is the air density; $1 - (w - w_e)/(w_0 - w_e)$ is the buoyancy correction for air; m is the molality; and w_e, w_0, and w are the weights of the empty, solvent-filled, and solution-filled pycnometer, respectively$\}$ were determined. Errors were calculated with the following equations:

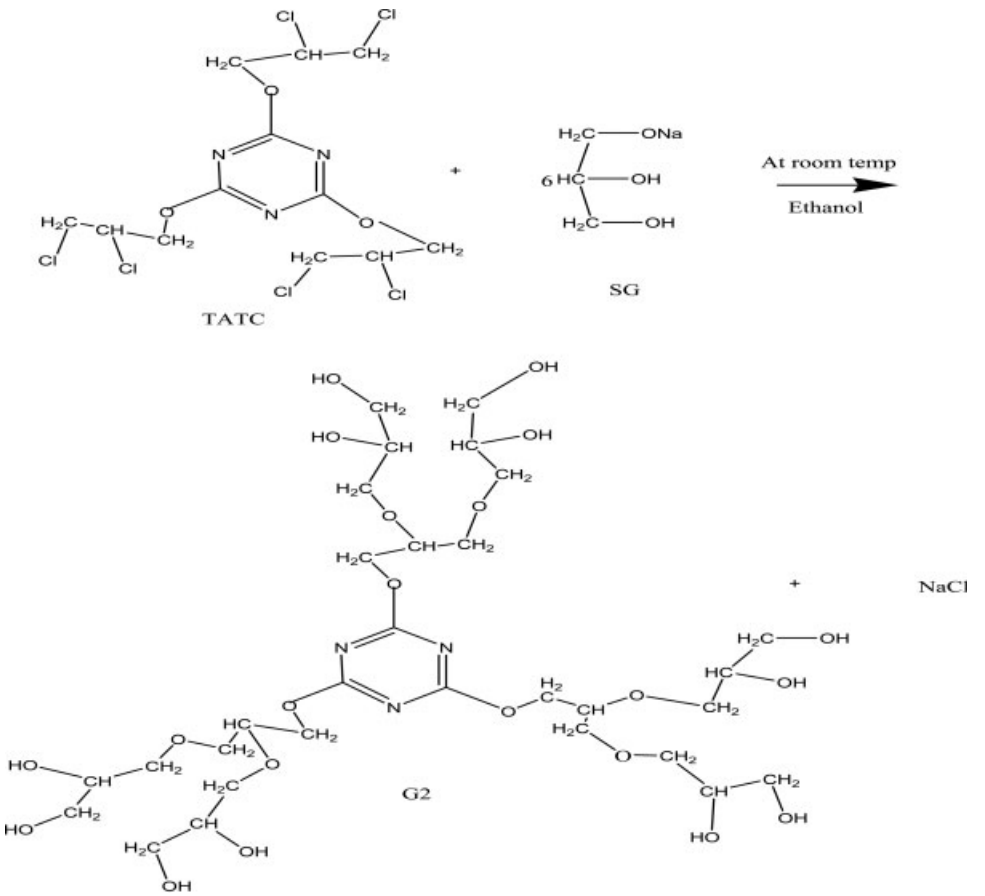

Figure 4 Preparation of G_2.

$$\sqrt{\left(\frac{w-w_0}{10^5}\right)^2+\left(\frac{w_e}{10^5}\right)^2} \approx \pm S_n$$

$$\sqrt{\left(\frac{w_0-w_e}{10^5}\right)^2+\left(\frac{w_e}{10^5}\right)^2} \approx \pm S_v$$

$$\sqrt{\left(\frac{\pm S_n}{w-w_e}\right)^2+\left(\frac{\pm S_v}{V_{pyk}}\right)^2} = \frac{\Delta\rho}{\rho}$$

where $V_{pyk} = (w_0 - w_e)/\rho_0$ is the pycnometer volume and $\Delta\rho$ is equal to $\rho - \rho_0$. The apparent molal volume (V_ϕ) was obtained as follows:

$$V_\phi = M/\rho + 1000/(\rho_0 - \rho)/\rho_0\rho m \quad (1)$$

where M is the molar mass. The uncertainty in V_ϕ was computed with eq. (2).

$$V_\phi = (1000/m)\Delta\rho/\rho \quad (2)$$

Regression analysis of the data

The ρ and V_ϕ data were least-square-fitted against m and extrapolated to $m = 0$ for their limiting values with the following equations:

$$\rho = \rho^0 + S_d m \quad (3)$$

$$V_\phi = V_\phi^0 + S_v m + S_v^* m^2 \quad (4)$$

where ρ^0 is the limiting density; S_d is the first-degree slope; V_ϕ^0 is the limiting apparent molal volume; and S_v and S_v* are the first- and second-degree slopes, respectively. V_ϕ^0 denotes the solute–solvent interactions, and S_v and S_v* denote the solute–solute interactions.

RESULTS AND DISCUSSION

Structural characterization

^{1}H-NMR spectroscopy

The ^{1}H-NMR spectra of G_1 and G_2 were recorded in deuterium on a Bruker Advance DPX-dix 300-MHZ spectrometer with D_2O as an internal reference. The ^{1}H-NMR spectra of SG, G_1, TATC, and G_2 are depicted in Figure 5. For SG, the signal at 3.817 ppm implies CH_2OH, whereas for CHOH, there is a multiplet from 3.599 to 3.685 ppm. A sharp signal at 4.713 ppm implies —CH_2—ONa. TGTA-I shows a singlet at 4.338–4.137 ppm that is equivalent to 1H, which indicates the —OH proton. Evidently, there is

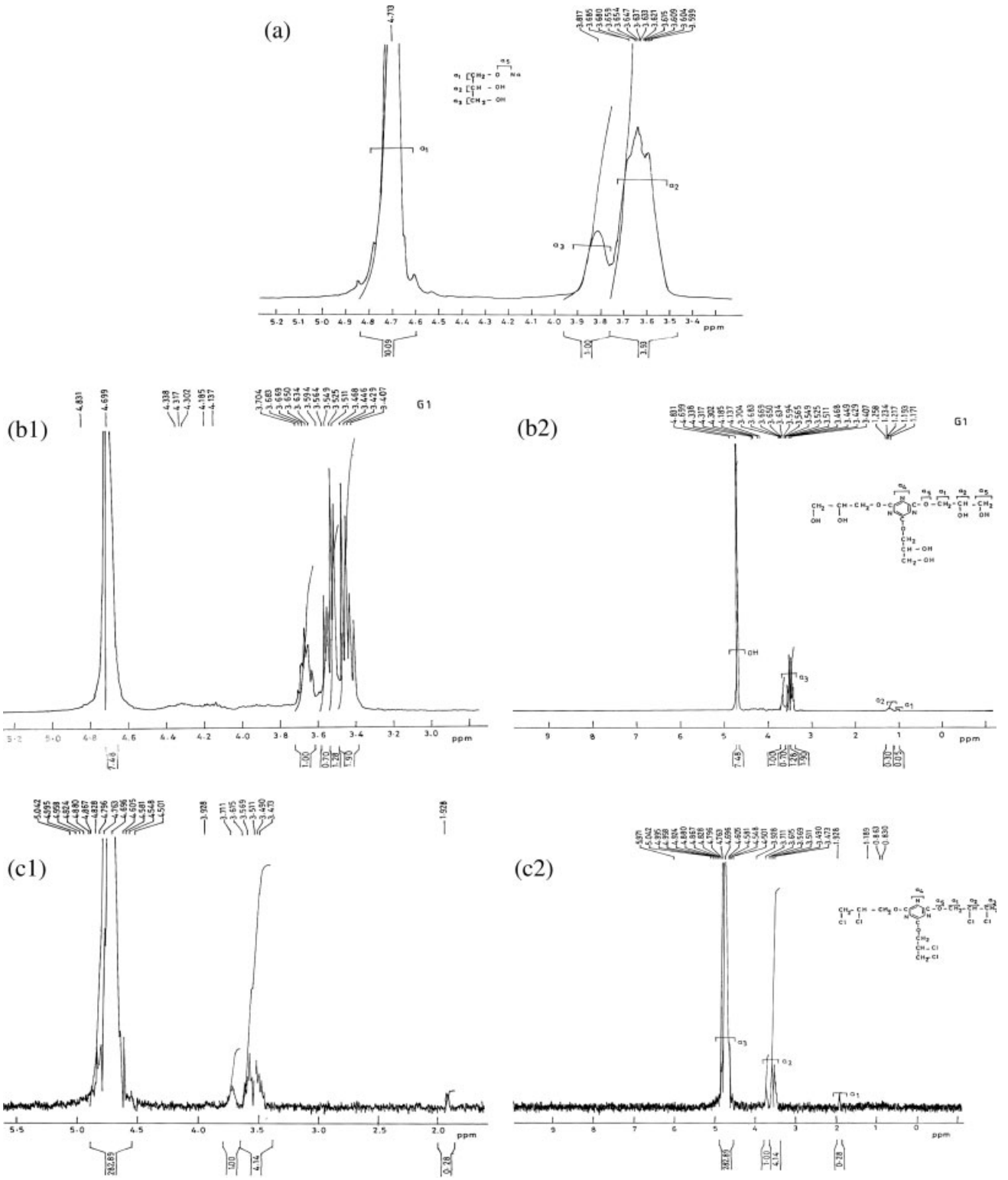

Figure 5 ^{1}H-NMR spectra of (a) SG, (b1) G_1, (b2) TATC, (c1) G_2, (c2) TATC, (d1) TATC, and (d2) G_2.

no coupling between the methylene proton and the proton of the —OH groups. A quartet centered at 3.407 ppm and also a singlet at 3.704 ppm, equivalent to 2H, exhibit the methylene protons, and they are shifted downfield because of bonding with oxygen, an electronegative atom. The ester group attached to the aromatic ring is shown by a signal at 4.699–4.831 ppm. The ^{1}H-NMR spectrum of TATC

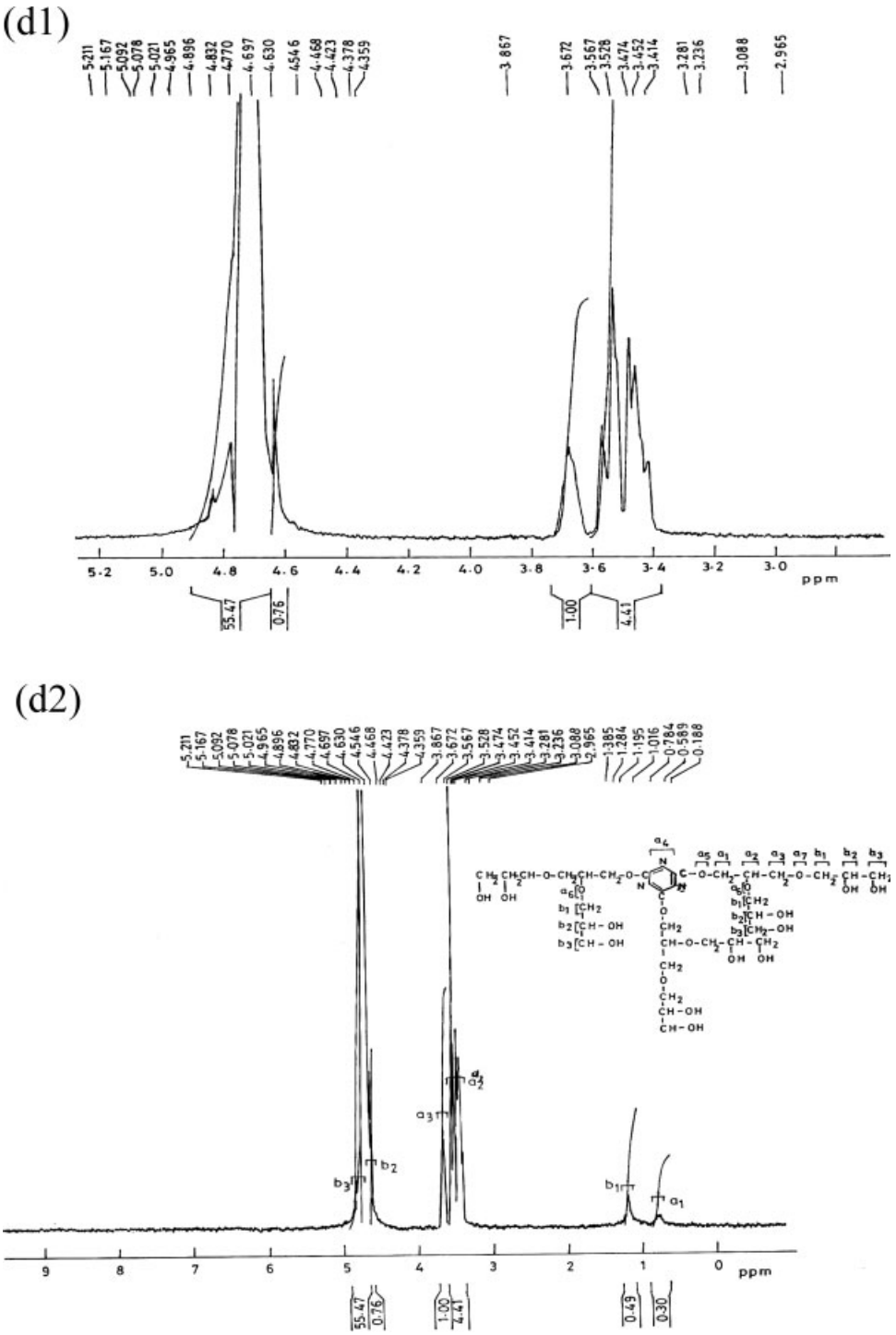

Figure 5 *Continued*

implies an ester group attached to the aromatic ring by a signal from 4.995 to 4.501 ppm, whereas a doublet at 1.89 ppm denotes the —O—CH_2 group. A doublet centered at 3.928 ppm, equivalent to 2H, implies the methylene proton. The methane proton, being adjacent to one chlorine atom, consequently shows a doublet centered at 5.971–5.042 ppm and equivalent to 1H, which represents the methane proton. A singlet at 3.711–3.615 ppm, equivalent to 2H, indicates the methyl proton, which is shifted downfield because it is bonded to oxygen, an electronegative atom. The ^{1}H-NMR spectrum of G_2 implies a singlet at 4.546 ppm equivalent to 1H, which indicates the OH proton; evidently, there is no coupling

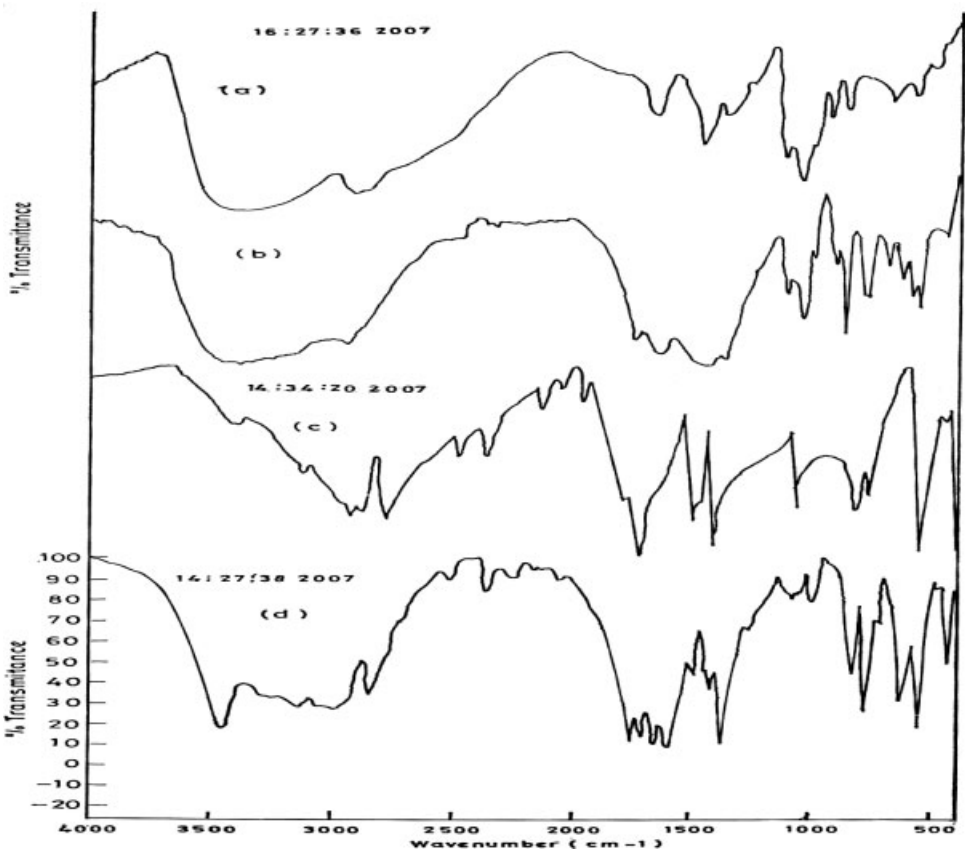

Figure 6 IR spectra of (a) SG, (b) TGTA, (c), TGTA chloride, and (d) G_2 dendrimer.

between the methylene protons and the protons of the OH group. A quartet centered at 3.672–3.5675 ppm, equivalent to 2H, implies the methylene protons, which are adjacent to an electronegative atom, showing resonance at a lower field. Aliphatic saturated ether is found at 3.672 ppm, whereas —C—OH sn-2 in glycerol is noted by a multiplet at 3.867 ppm, and —C—OH sn-3 in glycerol is noted by a doublet at 3.567–3.528 ppm. The bonded water is implied by a broad signal at 3.672 ppm. The ester group attached to the aromatic ring is noted by the signal at 4.546–5.092 ppm.

Fourier transform infrared spectroscopy

Fourier transform infrared with a Michelson scanning interferometer was used for structural elucidation. The resultant beam was divided at the beam splitter. Absorption bands shown on the phenylethylamine (PEA) IR spectrum correspond to PEA signals reported in the literature[12] and ^{1}H-NMR spectral signals registered in the literature. The IR spectrum [Fig. 6(a)] implies a deformed oxide group at 1200 cm^{-1} as a shoulder; the bands in the fingerprint region (926.40–1200 cm^{-1}) denote C—O bending, the band at 3371.04 cm^{-1} depicts the O—H stretching, the band at 2923.86 cm^{-1} indicates the C—H stretching, and the bands at 1456.95 cm^{-1} and 1653.62 cm^{-1} indicate the bending vibrations for the C—H groups. Because of the attachment of sodium, the C—O— stretching displaces to 1257.5 cm^{-1} with a broad band. SG is hygroscopic, and its IR spectrum shows the bonded water molecules in the region of 3100–3600 cm^{-1}. The IR spectrum of G_1 [Fig. 6(b)] consists of three polar zones having a lone pair of electrons at the nitrogen of azine, and this makes a hydrogen bond with oxygen of trace water with a broad band at 3385.66 cm^{-1} and O—H bending vibrations at 1448.26 cm^{-1}. The band at 2932.84 cm^{-1} shows C—H stretching, and the broad band at 2322.91 cm^{-1} indicates deformed C—H stretching due to the attached benzene ring. The band at 1742.05 cm^{-1} shows C—O—C stretching vibrations with hydrogen bonding with water molecules, whereas the bands at 1634.68 cm^{-1} show the >C=N stretching due to the >C=N—C bond (unsaturated) at 1373.13 cm^{-1} and >CN—C (saturated) at 1111.07 cm^{-1}. The stretching band at 1044.61 cm^{-1} implies —C—O— in TGTA, whereas in the fingerprint region, the substituted benzene ring shows out-of-plane

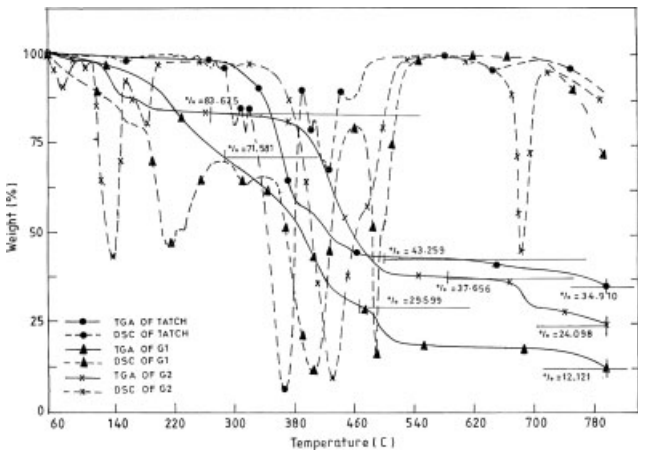

Figure 7 Thermogravimetric analysis (TGA) of the prepared products (DSC = differential scanning calorimetry).

bending vibrations at 994.11 cm^{-1}; below this, it makes the spectrum complicated. The IR spectrum of TATC [Fig. 6(b)] shows C—H stretching at 3115.78 cm^{-1} for CH_2—Cl and CH—Cl stretching from 813.05 to 763.69 cm^{-1}. The band at 1715.84 cm^{-1} shows C—O stretching of the ester group attached to the aromatic ring with a small shoulder at 3386.91 cm^{-1}, which implies stretching vibrations of hydrogen bonding at —C—O—CH_2 as well as bending vibrations at 1448.26 cm^{-1}. The band at 2924.95 cm^{-1} shows asymmetric C—H stretching, whereas a band at 2773.14 cm^{-1} shows symmetric C—H stretching of CH_2. The broad band shows deformed C—H stretching at 2471.74 cm^{-1} but >C=N stretching at 1491.35 cm^{-1}; the >C=N—C band (unsaturated) appears at 1345.83 cm^{-1}, and >CN—C (saturated) appears at 1132.56 cm^{-1}. The stretching band at 1060.36 cm^{-1} denotes —C—O— in TATC, whereas in the fingerprint region, the substituted benzene ring shows out-of-plane bending vibrations at 763.69 cm^{-1}; below this, it makes the spectrum complicated. The IR spectrum of G_2 [Fig. 6(d)] consists of 3 polar zones with a lone pair of electrons at the nitrogen of azine, and this makes a hydrogen bond with oxygen of trace water with a broad band at 3448.86 cm^{-1} and O—H bending vibrations at 1491.00 cm^{-1}. The band at 2995.16 cm^{-1} implies C—H asymmetric stretching, and the broad band at 2355.86 cm^{-1} indicates deformed C—H stretching, whereas a band at 2841.04 cm^{-1} shows symmetric C—H stretching of CH_2. The broad band at 2471.74 cm^{-1} shows deformed C—H stretching due to the attached benzene ring. The band at 1748.07 cm^{-1} shows C—O—C stretching vibrations with hydrogen bonding with water molecules at 3139.09 cm^{-1}, whereas the bands at 1654.02 cm^{-1} imply >C=N and stretching due to the >C=N—C bond (unsaturated) at 1373.23 cm^{-1} and >CN—C (saturated) at 1105.98 cm^{-1}. The stretching band at 1080.39 cm^{-1} implies —C—O— in TGTA, whereas in the fingerprint region, the substituted benzene ring shows out-of-plane bending vibrations at 988.10 cm^{-1}.

Thermogravimetric analysis

Thermograms were recorded with a Mettler Thermobalance TA-4000 system at a heating rate of 20°C/min from the ambient temperature to 780°C. The thermograms for the dendrimers at a scanning rate of 20°C/min are shown in Figure 7. Although a scanning rate of 10°C/min is always better, the heating range spans from the ambient temperature to 780°C; this is larger so the accuracy of a scanning rate of 20°C/min is informatory for our purposes. The characteristic temperatures for the assessment of the relative thermal stability, such as the initial decomposition temperature, temperature for 20% weight loss, temperature for the maximum rate of decomposition, and temperature for half-volatilization, are listed in Table I. A higher temperature for 20% weight loss implies greater thermal stability of a dendrimer. The thermal stability order of the dendrimers on the basis of the initial decomposition temperature is TCTA > G_1 > G_2, and a comparison of the temperatures for 20% weight loss for the dendrimers implies a decreasing order of stability of TCTA > G_2 > G_1, whereas a comparison based on the temperature for the maximum rate of decomposition for the dendrimers finds the order of TCTA

TABLE I
Activation Energy Calculated with Briodo's Method from the Thermogravimetric Analysis Graph of the Dendrimers

			T_{max} (°C)				Activation energy (kcal/mol)		
System	T_0 (°C)	T_{20} (°C)	Step I	Step II	Step III	T_S (°C)	Step I	Step II	Step III
G_1	86.00	237.14	287.82	467.06	796.26	392.90	16.56	10.10	13.66
G_2	82.00	308.60	267.90	584.22	796.26	464.30	15.87	19.09	11.22
TATC	265.0	343.00	499.87	797.43	—	405.80	27.97	17.58	—

T_0 = initial decomposition temperature; T_{20} = temperature for 20% weight loss; T_{max} = temperature for the maximum rate of decomposition; T_S = temperature for half-volatilization.

> G_1 > G_2. These observations of the thermal stability imply higher thermal stability for the dendrimers with chloride ions on the surface than for those with OH groups.[13] The activation energy was calculated with Briodo's method,[18] and it ranges from 11.22 to 27.97 kcal/mol for thermal decomposition. Hence, the thermal stability of the dendrimers is significantly related to the surface groups as well as branching components. It also shows an extent of moisture absorption from the atmosphere and hence can be used to determine the most suitable drying temperature of the dendrimers. The thermogram curve shows three reaction zones for G_1 and G_2 but two zones for TATC. With G_1, the three major reaction zones are as follows:

1. The region from 54.69 to 287.82°C shows a rupture of the ester as well as the —OH group with the formation of a water molecule. The IR broad band and a decrease in weight at 54.69°C imply unbound water.
2. The region from 287.82 to 467.06°C shows a rupture of C=O that results in the formation of CO, leaving behind only a core. The curve shows more than 80% degradation in the weight.
3. The region from 467.06 to 796.26°C shows oxidative degradation of the triazine ring, which results in —C≡N, and furthermore, the molecule degrades completely.

G_2 also contains three main reaction zones.

1. The region from 52.34 to 267.90°C shows a rupture of the ester as well as the —OH groups with the formation of a water molecule. The IR broad band and a decrease in weight at 52.34°C imply unbound water.
2. The region from 267.90 to 584.22°C shows a zone of C=O formed by a transfer of H^+ ions, which results in a stabilized intermediate with the formation of CO. The molecule loses a major portion (70%) of its weight in this region.
3. The region from 584.22 to 796.26°C, like that of TGTA-I, shows oxidative degradation of the triazine ring, which results in —C≡N, after which the molecule degrades completely.

Unlike G_1 and G_2, TATC contains only two zones.

1. The region from 53.51 to 499.87°C is the major degradation region in the thermogram with 60% weight loss. Here the rupture of the Ar—O—CH_2 group as well as the C—Cl bond occurs and results in Cl_2 and CO.
2. The region from 499.87 to 797.43°C, like that of G_1 and G_2, shows oxidative degradation of the triazine ring, which results in —C≡N with complete degradation.

Physicochemical characterization

The G_2 > TATC > SG > G_1 > TCTA sequence of ρ^0 for binary systems at 298.15 K (Table II) with a stronger internal pressure in solutions is due to stronger hydrophilic interactions and van der Waals forces. The ρ^0 values, higher than that of water, imply stronger hydrogen bonding with water because the hydrogen-bonded water is disrupted, interacting strongly with SG, G_1, G_2, and TATC but not TCTA, which is a water-structure breaker. This shows stronger structural interactions for G_2 than for TATC, SG, and G_1 but weaker interactions of TCTA with water because of the 3-Cl group (Fig. 3). Comparatively, the TATC > TCT > G_1 > SG > G_2 order of S_d values implies stronger activity of TATC with weaker TATC–TATC intermolecular interactions, and this is the reverse behavior of ρ^0. The S_d values of TATC signify larger structural reorientation (Table III) due to destabilization with the composition, which favors stronger TATC–TATC hydrophobic intermolecular interactions with higher internal pressure. The TATC–TATC interactions weaken the electrostriction of water with mild water–dendrimer interactions. Second electrostatic changes could favor cage formation around the TATC molecule, applying higher internal pressure with stronger hydrophobic interactions. Strategically, the intermolecular engineering of a dendrimer is of biotechnological, biomedical, and biophysical use with respect to the medium and physical conditions. The lower S_d values for G_2 imply weaker effects of compositions on G_2–G_2 interactions, so the hydrated G_2 molecules may not further destabilize the water because of stabilization of the structure-breaking action. The V_ϕ^0 values of the aqueous systems are in the order of TATC > G_2 > G_1 > TCTA > SG with the concentration at 298.15 K, with the reverse trend for ρ^0 values. A negative contribution to V_ϕ^0 of SG is due to stronger interactions between Na^+ and strongly polarized hydrogen of the solvent.[19–21] The positive contribution to V_ϕ^0 of TCTA, G_1, G_2, and TATC is due to hydrophilic–hydrophilic interactions, as reported by Singh et al.[22] The G_2 > SG > G_1 > TCTA > TATC order of the S_v values falls in the range of -2.83×10^2 to $1.14 \times 10^4/10^{-6}$ kg m^3/mol^2, with larger expansion in the size of the confirmatory state.[23] This fascinated us because the V_ϕ^0 values imply cage formation of a larger size around the dendrimer molecules, although it is contradictory vis-à-vis the ρ^0 values. Because of intermolecular forces between TATC and water and in water

TABLE II
η, η_r, η_{sp}, η_{red}, η_{inh}. γ, $1/m(2.303)\log \eta_r$, and v/V Values for SG, TCTA, G_1, TATC, and G_2 at 298.15 K

m (mol/kg)	η (0.1 kg m^{-1} s^{-1})	η_r	η_{sp}	η_{red} (kg/mol)	η_{inh}	γ (10^{-4} J/m^2)	$1/m(2.303)\log \eta_r$	v/V
SG								
0.01	0.8973	1.0078	0.0078	0.7846	0.0088	72.28	0.7817	0.3138
0.02	0.9055	1.0171	0.0171	0.8533	0.0190	71.78	0.8463	0.3413
0.04	0.9240	1.0379	0.0379	0.9464	0.0417	71.30	0.9291	0.3785
0.06	0.9441	1.0604	0.0604	1.0063	0.0659	70.82	0.9773	0.4025
0.08	0.9651	1.0841	0.0841	1.0508	0.0907	70.36	1.0092	0.4203
TCTA								
0.01	0.8967	1.0072	0.0072	0.7151	0.0080	72.43	0.7127	0.2860
0.02	0.9064	1.0180	0.0180	0.9024	0.0201	71.97	0.8945	0.3610
0.04	0.9258	1.0399	0.0399	0.9970	0.0439	71.08	0.9778	0.3988
0.06	0.9453	1.0618	0.0618	1.0293	0.0673	70.76	0.9989	0.4117
0.08	0.9648	1.0837	0.0837	1.0461	0.0903	70.34	1.0048	0.4184
G_1								
0.01	0.8964	1.0068	0.0068	0.6800	0.0076	72.80	0.6778	0.2720
0.02	0.9058	1.0174	0.0174	0.8723	0.0194	71.75	0.8649	0.3489
0.04	0.9266	1.0408	0.0408	1.0198	0.0449	70.76	0.9997	0.4079
0.06	0.9548	1.0724	0.0724	1.2068	0.0785	69.79	1.1653	0.4827
0.08	0.9814	1.1023	0.1023	1.2793	0.1095	69.34	1.2182	0.5117
G_2								
0.01	0.9154	1.0282	0.0282	2.8210	0.0313	72.45	2.7824	1.1284
0.02	0.9421	1.0582	0.0582	2.9102	0.0636	71.93	2.8291	1.1641
0.04	1.0000	1.1232	0.1232	3.0807	0.1306	70.90	2.9057	1.2323
0.06	1.0608	1.1915	0.1915	3.1921	0.1969	69.91	2.9211	1.2768
0.08	1.1238	1.2623	0.2623	3.2786	0.2617	69.43	2.9121	1.3114
TATC								
0.01	0.9152	1.0279	0.0279	2.7927	0.0309	72.93	2.7549	1.1171
0.02	0.9403	1.0562	0.0562	2.8087	0.0614	71.94	2.7332	1.1235
0.04	0.9923	1.1145	0.1145	2.8635	0.1218	71.58	2.7116	1.1454
0.06	1.0468	1.1758	0.1758	2.9294	0.1819	71.22	2.6991	1.1717
0.08	1.1033	1.2392	0.2392	2.9900	0.2409	70.87	2.6813	1.1960

itself, such changes in the molecular size are attributed to changes in the dipole moment. A larger expansion in the TATC volume with the composition implies slightly stronger volumetric interactions with weaker hydrophilic forces in comparison with other systems. An expansion of V_ϕ^0 for G_2 predicts an unfolding of the structure with a higher activation energy[24] (Table I) and is fitted in a polynomial against the concentration, predicting different intermolecular interactions around lower, medium, and higher concentrations. The $G_2 > G_1 >$ SG >TCTA > TATC and TCTA > G_1 > SG > G_2 orders of S_v and S_v* are the reverse of each other, with stronger intermolecular interactions for higher compositions, which predict more opening of the tertiary structures (Fig. 4). S_v* of TCTA at a higher concentration shows larger expansion, and G_2 shows the least, with values ranging from -1.19×10^5 to $+ 2.37 \times 10^4/10^{-6}$ kg^2 m^3/mol^3.

TABLE III
V_ϕ^0 Values Along with S_v and S_v* Values Obtained by the Regression of V_ϕ^0 Data Against m at 298.15 K

System	V_ϕ^0 (10^{-6} m^3/mol)	S_v (10^{-6} m^3 kg^{-1} mol^{-2})	S_v* (10^{-6} m^3 kg^{-2} mol^{-3})
SG	− 129	6,196.40	− 48,626.00
TCTA	229	− 3,025.97	23,671.00
G_1	52,177	3,412.67	− 39,758.45
G_2	281,872	11,368.39	− 119,025.62
TATC	279,280	− 28,288.48	—

η

η was calculated as follows:

$$\eta = \eta_0(\rho t)/(\rho_0 t_0) \quad (5)$$

where t and t_0 are the flow times and η and η_0 are the viscosities of the solution and solvent, respectively. The relative viscosity (η_r) was calculated with η/η_0; the specific viscosity (η_{sp}) was calculated as follows:

$$\eta_{sp} = (\eta/\eta_0) - 1 \quad (6)$$

The inherent viscosity (η_{inh}) was calculated with eq. (7), which presents the ratio of the natural logarithm of η_r to the mass concentration (m):

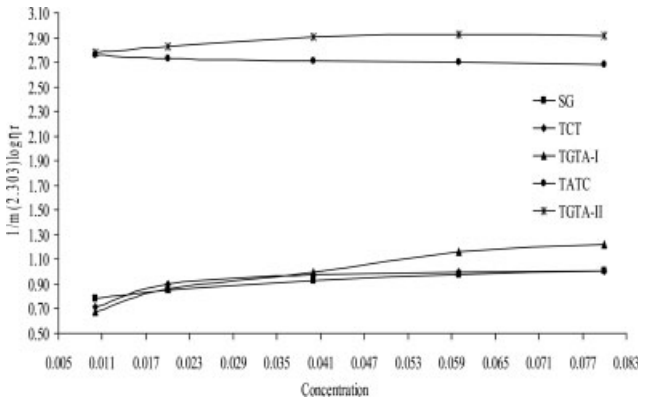

Figure 8 Plots of the reduced viscosity (kg/mol) versus the concentration (mol/kg) for the dendrimer in an aqueous solution at 298.15 K.

$$\eta_{inh} = \ln \eta_r / m \tag{7}$$

[η] was calculated with the following relation.

$$[\eta] = \lim_{m=0}, \eta_{sp}/m = 1/m(2.303) \log \eta_r \tag{8}$$

where m is the concentration (w/w) in 1000-g solutions. The plots of η_{sp}/m and $1/m(2.303)\log\ \eta_r$ versus m are linear (Figs. 5 and 8). This illustrates similarities in the properties of the dendrimers and those of the polymeric molecules.[25] Negative slopes of $1/m(2.303)\log\ \eta_r$ versus m (Fig. 5) further predict dendrimers near the polymer with respect to the structure and properties. The data can be used to estimate a rational relation between the volumes and molecular weights; thus, the monomer of our dendrimers along with markers shows properties like those of macromolecules in aqueous solutions. Thus, the Mark–Houwink–Sakurada equation[26] is relevant for molecular weight determination:

$$[\eta] = kM^a \tag{9}$$

where k and M are empirical parameters characteristic of the dendrimers and solvent. However, for infinitely large dendrimers, Frechet et al.[27] reported certain restrictions for the use of this equation. A logarithm of the relation is given in the equation to evaluate the k and a constants through the plotting of log [η] values of chosen markers against the molecular weight (M):

$$\log[\eta] = \log k + a \log M \tag{10}$$

where a and k are 0.2645 and 0.0174, respectively. Reportedly, the a value for much coiled, rigidly rodlike molecules ranges from 0.5 to 1.7. Flory and Leutner[28] found k and a values of 2.0×10^{-4} and 0.76, respectively (Table IV), using monodispersive specimens of bovine serum albumin, egg albumin, and lysozyme of different molecular weights.

TABLE IV
R_G and Molecular Weight Values of SG, TCT, G_1, TCTA, and G_2 at 298.15 K

System	log M	M_w	k (cm^3/gm)	a	R_G
SG	—	114	—	—	72.24
TCTA	—	184.41	—	—	89.00
G_1	4.63092	52,300.0	0.0002	0.76	586.37
G_2	5.45136	282,748.0	0.0002	0.76	1578.13
TATC	5.44632	279,447.0	0.0002	0.76	1567.35

M_w = weight-average molecular weight.

Regression of the viscosities

Krigbaum-Wall[29] and Cragg-Bigelow[30] noted the reduced viscosity (η_{sp}/m) values in a linear relation with the concentration, and they were supported by the Huggins equation:

$$\eta_{sp}/m = [\eta] + Bm \tag{11}$$

where $B = KH[\eta]^2$ and $[\eta] = \lim_{c\to 0}(\eta_{sp}/c)$; m, B, and KH are the concentration, viscometric interaction parameter, and Huggins constant, respectively. The η_{sp}/m values were fitted with eq. (11). η_{sp}/m versus the concentration for the dendrimers shows a linear relation (Fig. 8). Both [η] and B were obtained (Table V) with extrapolation to the zero concentration. The $G_2 > TATC > G_1 > TCTA > SG$ sequence for the [η] values implies a larger decrease with the

TABLE V
ρ^0, [η], [η_{inh}], γ^0, S_d, B, B', and $S_t m$ Values Obtained by the Regression of ρ, η_{red}, η_{inh}, and γ Data Against m at 298.15 K

	ρ^0 (10^{-3} kg/m^3)	S_d (10^3 kg^2 m^{-3} mol^{-1})	[η] (0.1 kg/mol)	B [slope; (0.1 kg/mol)^2]	[η_{inh}] (0.1 kg/mol)	B' (0.1 kg/mol)	γ^0 (10^{-4} J/m^2)	$S_t m$ (kg^2 mol^{-1} s^{-2})
SG	0.99874	0.03120	0.6615	3.7442	0.7749	3.1858	72.140	− 26.230
TCTA	0.99621	0.05893	0.7645	4.1301	0.7677	3.5733	72.560	− 29.510
G_1	0.99843	0.03174	0.7710	8.3365	0.6708	7.4840	72.920	− 48.330
G_2	1.00121	0.01353	2.7801	6.5816	2.7215	1.8748	72.792	− 44.445
TATC	0.99943	0.11378	2.7557	2.8851	2.7678	− 0.9868	72.796	− 25.830

TABLE VI
Radius and Barrier Energy Values of SG, TCTA, G_1, TATC, and G_2 at 298.15 K

	SG		TCTA		G_1		TATC		G_2	
m (mol/kg)	Radius (Å)	Barrier energy ($\times 10^{-23}$ J)	Radius (Å)	Barrier energy ($\times 10^{-23}$ J)	Radius (Å)	Barrier energy ($\times 10^{-23}$ J)	Radius (Å)	Barrier energy ($\times 10^{-23}$ J)	Radius (Å)	Barrier energy ($\times 10^{-23}$ J)
0.01	2.04	12,812.83	2.33	12,812.706	15.03	12,812.644	42.09	12,816.36	42.40	12,816.405
0.02	2.10	12,938.351	2.51	12,938.524	16.33	12,938.418	42.17	12,945.10	42.84	12,945.438
0.04	2.18	13,065.862	2.60	13,066.21	17.21	13,066.366	42.44	13,078.60	43.66	13,079.991
0.06	2.22	13,142.173	2.63	13,142.405	18.20	13,144.188	42.76	13,160.63	44.18	13,163.015
0.08	2.25	13,197.542	2.64	13,197.479	18.56	13,200.53	43.06	13,221.45	44.58	13,224.748

composition changing from 0.0065 to 1.9847 $\times$ 10^{-3} kg/mol. This shows a decrease in [η] with the concentration for G_2, with a larger hydrodynamic volume than that of the others with an effective conformational structure. This shows greater dependence of the stability of the hydrodynamic size of a hydrated complex on the thermal energy. The [η] values for SG are lower than those for others with weaker Newtonian forces on the viscous flow because of weakly stable H_2O–SG hydrogen bonding. However, the [η] values of G_2 are higher than those of others by 0.02441, 2.0091, 2.0156, and 2.1456 $\times$ 10^{-3} kg/mol (Table II), with reverse behavior of the B values.[31] The criterion at $[\eta_A]_B = [\eta_A]_B - [\eta_B]$ for the dendrimer–triazine method was used for the dendrimer–triazine compatibility, as reported elsewhere.[32] If $[\eta_A]_B > 0$, then dendrimers A and triazine B are compatible, whereas $[\eta_A]_B < 0$ implies that dendrimers A and triazine B are incompatible. Accordingly, G_1, G_2, and TATC are compatible (0.0065, 2.1012, and 2.1256 kg/mol).

$1/m(2.303)\log \eta_r$ versus m

Plots of $1/m(2.303)\log \eta_r$ versus m (Fig. 5) show a linear relation due to an effect of the structure of the dendrimer and markers on the water structure, with G_2 greater than G_1 (Table II). The $1/m(2.303)\log \eta_r$ limits and slopes for G_1 are considerably lower and higher than those for G_2, with greater molecular motion for the stabilization of water–dendrimer complexes, indicating the frictional forces affected by the concentration. The markers show positive slopes with a best dependence of $1/m(2.303)\log \eta_r$. Their D values are positive; perhaps chloride and —OH groups influence the frictional forces at higher concentrations.[32,33]

[η_{inh}]

The [η_{inh}] value is associated with the shape and size and is very low (Table V). Like ρ^0, [η_{inh}] implies weaker heteromolecular forces with water. However, very high B' values indicate a very high influence of the composition on heteromolecular forces. Perhaps the composition considerably influences Newtonian flow and rotational motions of molecules. The markers show an order of reaction in terms of [η_{inh}] as follows: bovine serum albumin > egg albumin > lysozyme. However, the B' values are higher than those of the dendrimers, the integrity of the hydrodynamic spheres being strengthened with the composition of the markers. The activation energies are in the order of G_2 > TCTA > G_1 at 298.15 K because of molecular resistance to viscous flow due to unexpected very high rotations and reorientations. Thus, the activation energy depicts innumerable reorientations, electronic motions, and vibrations of glycerate. The spherical G_1 dendrimer with three branches of glycerate develops higher Newtonian forces or stronger frictional/torsional forces on adjacent layers of laminar flow. These forces increase many times for G_2 generation, which shows greater rotational and electronic rearrangement due to the greater activation energy and B' values of the molecules. The [η_{inh}] and [η] values for G_2 are slightly higher than those of G_1 with flow dynamics similar to those of G_2. Hence, the larger the branching is, the higher the hydrodynamic volume is.

Barrier energy of the dendrimer molecules

The barrier energy was computed by Eyring's method with the η values from the equation:

$$\text{Barrier energy} = kT(\log[\eta] - \log m - \log h) \qquad (12)$$

where m is the concentration (mol/cm^3), k is Boltzmann's constant, T is the absolute temperature, and h is Planck's constant (Table VI).

Radius of the dendrimer molecules

The radius was calculated with the Einstein equation:

TABLE VII
Experimental and Literature Values of ρ, V_ϕ, and η at 303.15 K

		ρ± (10^3 kg/m^3)		V_ϕ± (10^{-6} m^3/mol)		η± (0.1 kg m^{-1} s^{-1})	
	g %	Literature	Experimental	Literature	Experimental	Literature	Experimental
Bovine serum albumin	0.0010	0.99641	0.99642	64,907.39	64,907.41	0.7895	0.7894
	0.0014	0.99622	0.99621	65,070.20	65,070.19	0.7992	0.7993
	0.0018	0.99619	0.99619	65,116.27	65,116.27	0.8085	0.8085
Egg albumin	0.0010	0.99625	0.99625	39,890.08	39,890.08	0.7614	0.7614
	0.0014	0.99623	0.99622	39,970.16	39,970.14	0.7769	0.7770
	0.0018	0.99623	0.99623	40,010.54	40,010.54	0.7917	0.7917
Lysozyme	0.0010	0.99634	0.99633	39,850.97	39,850.95	0.8039	0.8040
	0.0014	0.99621	0.99621	39,977.65	39,977.65	0.8041	0.8041
	0.0018	0.99607	0.99607	40,054.00	40,054.00	0.8065	0.8065

The data were taken from ref. 19.

$$\eta_{sp} = (10\pi r^3 m_c)/3m \tag{13}$$

where r is the radius of the spherical molecule, m is the mass, and m_c is the mass concentration. Thus, by this simple theory, η_{sp} is predicted to be linear versus m_c.

Radius of gyration (R_G) of the dendrimers

For many synthetic polymers, the chains tend to adopt a tight, ball-like configuration in solution, and an average structure is defined by R_G:

$$R_G^3 = ([\eta]M)/K' \tag{14}$$

where M is the molar mass and K' is a constant. For a polymer with a random-coil conformation, the theory predicts that $R_G \propto M^{1/2}$. It predicts a dependence of [η] on M as follows:

$$[\eta] = K'M^{1/2} \tag{15}$$

This is applied to polymer solutions under what are known as theta conditions.[34]

Shape determination

The shape of our dendrimers was determined as follows:

$$\eta_{sp} = (\eta/\eta_0) - 1 = 2.5v/V \tag{16}$$

where v is the volume occupied by all the spheres and V is the total volume of the solution in the viscometer bulb. Einstein[35] reported $v/V < 2.5$ for spherical particles and $v/V > 2.5$ for nonspherical particles. For dendrimers, v/V is less than 2.5 (Table VII) and remains almost constant. Hence, the dendrimers are spherical in shape, with no change in the viscous flow without any preferential orientation. v/V is a dimensionless value, as mentioned in eq. (15). Our experimental values (Table VII) fall in the range of 0.2810–1.3114 for SG, TCTA, G_1, TCTA, and G_2 for concentrations ranging from 0.01 to 0.08 mol/kg. This implies no stable conformation in the dendrimer geometry. Contrary to the v/V values of G_1, the values for G_2 (Fig. 4) are slightly higher with almost similar trends, with a slightly higher increase with the concentration, whereas the magnitude for both dendrimers remains less then 2.5 because of the consistency in the shape. The chains are propagated in a mathematical manner, bifurcating into two chains, and the shape remains spherical, forming a denser and more complicated structure.

Surface tension analysis

γ was calculated as follows:

$$\gamma = (n^0\rho\gamma^0)/(n\rho^0) \tag{17}$$

where n^0 and n are the drop numbers of the solvent and solution, respectively; ρ and ρ^0 have the usual meanings; and γ^0 is the surface tension of water. The γ data were least-square-fitted against and extrapolated to $m = 0$ for limiting values from the following equation:

$$\gamma = \gamma^0 + S_t m \tag{18}$$

where γ^0 is the limiting surface tension and S_t is the slope, whose values for SG, TCTA, G_1, G_2, and TATC are higher than that of water by 0.27, 0.42, 0.78, 0.656, and 0.652 × 10^{-2} N/m, respectively. This indicates stronger surface forces than those of water due to stronger hydration spheres around the dendrimer molecules. The values are in the order of G_1 > TATC > G_2 > TCTA > SG, and G_1 and G_2 differ from the order of V_ϕ^0 and η^0 values. γ^0 elucidates a

state of cohesive and adhesive forces rather than electrostatic and Newtonian forces,[36] whereas the orders of values of TATC, TCTA, and SG are the same as those of V_ϕ^0 and η^0. γ increases with the concentration; however, the increase becomes much lower after a critical concentration. Hence, γ of SG is lower than that of TCTA, G_1, G_2, and TATC at the same concentration. Thus, the surface activity of SG is higher than that of TCTA, G_1, G_2, and TATC because of the slightly stronger ionic nature of SG molecules versus that of TCTA, G_1, G_2, and TATC.

CONCLUSIONS

The surface functions of dendrimers control their properties, and the dendritic encapsulation of functional molecules allows the isolation of the active site. The structure mimics a structure of active sites in biomaterials because dendritic scaffolds separate internal and external functions. A dendrimer can be water-soluble when its end group is a hydrophilic group such as —OH. It is possible to design a water-soluble dendrimer with internal hydrophobicity, which would allow it to carry hydrophobic materials in its interior. The dendrimer (redox-active nanoparticles) can be synthesized with the redox molecules between the nanoparticle cores and the dendritic wedges; despite their isolation, some of the redox molecules (CH_2OH) remain uncoupled and thus still reactive. An increase in η and a decrease in V_ϕ have been noted. The dendrimers are efficient drug delivery systems for sending medications to the affected part inside a patient's body directly. The presence of diols at the end chains of a dendrimer assist it in encapsulating gold nanoparticles, which are profoundly useful in photothermal therapy and imaging.

The authors are very thankful to A. P. Raste, Principal of Deshbandhu College, for his infrastructural support.

References

1. Tomalia, D. A.; Starbrush, T. M. Aldrichimica Acta 1993, 26, 91.
2. Newkome, G. R.; Yao, Z. Q.; Baker, G. R.; Gupta, V. K. J Org Chem 50, 2003, 2006.
3. Tracki, L. A. Thermodynamics and Rheology; Hanser: Munich, 1989.
4. Frechet, J. M. J. Science 1994, 263, 1710.
5. Newkome, G. R.; Weis, C. D.; Moorefield, C. N.; Baker, G. R.; Childs, B. J.; Epperson, J. Angew Chem Int Ed 1998, 37, 307.
6. Melad, O. Asian J Chem 2002, 14, 849.
7. Mourey, T. H.; Turner, S. R.; Rubenstein, M.; Frechet, J. M. J.; Hawker, C. J.; Wooley, K. L. Macromolecules 1992, 25, 2401.
8. Olabisi, O.; Robeson, L. M.; Shaw, T. Polymer–Polymer Miscibility; Academic: New York, 1979.
9. Singh, M.; Sharma, Y. K. Phys Chem Liq 2006, 44, 1.
10. Singh, M. J Appl Polym Sci 2004, 92, 3437.
11. Singh, M.; Kumar, A. J Sol Chem 2006, 35, 567.
12. Wahab, M. A.; Ali, M. A.; Mottaleb, M. A. Bull Kor Chem Soc 2002, 23, 953.
13. Singh, M. J Chem Thermodyn 2006, 39, 240.
14. Singh, M. J Biochem Biophys Methods 2006, 67, 151.
15. Jencks, W. P. Catalysis in Chemistry and Enzymology; Dover: New York, 1969.
16. Zhu, P. P.; Wang, P. Eur Polym J 1997, 33, 411.
17. Singh, M.; Pandey, M.; Yadav, R. K.; Verma, H. S. J Mol Liq 2007, 135, 188.
18. Noggle, J. H. Physical Chemistry, 3rd ed.; Addison-Wesley-Longmans: Reading, MA, 1996; p 479.
19. Singh, M.; Chand, H.; Gupta, K. C. Chem Biodiv 2005, 2, 809.
20. Singh, M.; Kumar, S. J Appl Polym Sci 2004, 93, 47.
21. Singh, M.; Gupta, S. Phys Chem Liq 2007, 45, 281.
22. Danielewicz-Ferchmin, I.; Ferchmin, A. R. Phys Chem Chem Phys 2004, 6, 1332.
23. Singh, M.; Chauhan, S. J Appl Polym Sci 2007, 104, 3261.
24. Danait, A.; Deshparrde, D. D. Eur Polym J 1955, 31, 1221.
25. Melad, O.; Baraka, R.; Salem, J. K. J.; Hilles, H.; Ei-Khazendar, A. Chin J Polym Sci 2003, 21, 15.
26. Carey, B. S.; Scriven, L. E.; Davis, H. T. AIChE J 1980, 26, 705.
27. Singh, M. Surf Interface Anal 2007, 14, 973.
28. Evans, H. B., Jr.; Clever, H. L. J Phys Chem 1964, 68, 3433.
29. Gambill, W. R. Chem Eng 1958, 143.
30. Gao, G. Fluid Phase Equilib 1992, 74, 85.
31. Singh, M.; Kumar, V. Int J Thermodyn 2007, 10, 121.
32. Lam, V. T.; Benson, G. C. Can J Chem 1970, 48, 3773.
33. Singh, M. J Appl Polym Sci 2007, 103, 1420.
34. Schmidt, R. L.; Randall, J. C.; Clever, H. L. J Phys Chem 1966, 70, 3912.
35. Hemant, S.; Patel, N. B.; Patel, K. C.; Patel, I. Polym J 2005, 14, 1090.
36. Singh, M.; Gupta, S. Synth Commun, to appear.